Brain Research xxx (xxxx) xxx

Contents lists available at ScienceDirect

Brain Research

journal homepage: www.elsevier.com/locate/brainres

Research report

Mobilisation and redistribution of multivesicular bodies to the endfeet of reactive astrocytes in acute endogenous toxic encephalopathies

Tatyana Shulyatnikova [*], Vladimir Shavrin [1]

Zaporizhzhia State Medical University, Department of Pathological Anatomy and Forensic Medicine, Zaporizhzhia, Mayakovsky Avenue, 26, 69035, Ukraine

ARTICLE INFO

Keywords:
Astroglia
Sepsis-associated encephalopathy
Acute hepatic encephalopathy
Multivesicular bodies
Exosomes
Blood brain barrier

ABSTRACT

Endogenous toxicity caused by systemic inflammation as well as by acute liver failure triggers a wide range of dysfunctional disorders in the brain ranging from delirium and acute psychosis to coma. Astrocytes, the main homeostatic cells of the central nervous system (CNS), play a key role in pathophysiology of neurotoxic insults. We examined the cecal ligation and puncture (CLP) and acetaminophen-induced liver failure (AILF) of Wistar rats, and analysed ultrastructure of astrocytes in the brain cortex and subcortical white matter of sensorimotor zone with transmission electron microscopy. Both models showed significant similarities in reactive changes of astroglial endosomal machinery. In survived animals (with relative prevalence in the CLP-model), at 24 h after intervention we found an increase in number of multivesicular bodies (MVBs) in astroglial perikarya and astroglial processes. In particular, the number of MVBs substantially (3 times of control values) increased in the perivascular astroglial endfeet. Increased number of MVBs in astrocytes was associated with the lesser degree of intracellular oedema and with signs of compensated oedematous tissue changes. In deceased animals, up to 24 h after intervention, single MVBs were localised mainly in astroglial perikarya, and their number was not significantly changed compared to control. Activation of astroglial endosomal-exosomal machinery in both models reflects the uniform pattern of reactive changes of astroglia in these two systemic conditions and may represent activation of astroglial defence in sepsis-associated encephalopathy (SAE) and acute hepatic encephalopathy (AHE). Our data highlight the special role of astroglial adaptive activity in the counterbalancing of an impaired brain homeostasis under action of endogenous toxins. Accumulation of MVBs in astrocytic processes indicates the activation of their intercellular and gliovascular interactions through endo- and exocytosis in SAE and AHE.

1. Introduction

Intoxication is a frequent component of multiple organ dysfunction syndrome (MODS). Sepsis and liver damage are among the most common somatic pathologies, accompanied with a secondary endogenous toxicity (Jain et al., 2012; Ronco et al., 2010). In the etiological structure of sepsis, abdominal sepsis, which is a complication of intra-abdominal infection, is arguably the most frequent entity (Sartelli et al., 2015). Primary acute liver failure (ALF) usually accompanies acute infectious hepatitis and hepatosis, including toxic injury produced by hepatotoxic poisons (Montrief et al., 2019; Munoz, 2014). Endogenous intoxication involves the systemic action of numerous aggressive factors, including endotoxin itself (lipopolysaccharide, LPS), high levels of blood ammonia etc. (Brown, 2019; Jain et al., 2012; Shulyatnikova and Shavrin, 2017). The central nervous system (CNS), although controlling body detoxification systems and regulating homeostatic balance, remains insufficiently protected from the damaging effects of these factors, and against this background, acute brain dysfunction is a frequent component of MODS.

Acute brain dysfunction caused by sepsis-associated encephalopathy (SAE) complicates the course of sepsis (including its abdominal variant) in almost 70% of cases (Lamar et al., 2011; Sartelli et al., 2015; Shuliatnikova and Shavrin, 2018). The SAE results from multifactorial events, such as high systemic level of bacterial pathogens and the “cytokine storm”, all causing damage to the brain barriers and instigating a breakdown of brain homeostasis - leading to cognitive abnormalities (Shulyatnikova and Verkhratsky, 2020; Sonneville et al., 2013). Acute hepatic encephalopathy (AHE) manifests similarly as acute cerebral dysfunction and usually occurs in severe form, accompanied by an increased intracranial pressure, brain oedema and hepatic coma. The

* Corresponding author.
E-mail address: shulyatnikova.tv@gmail.com (T. Shulyatnikova).
[1] Professor Shavrin V.A. sadly passed away on 30 August 2020.

https://doi.org/10.1016/j.brainres.2020.147174
Received 12 August 2020; Received in revised form 27 September 2020; Accepted 20 October 2020
Available online 24 October 2020

pathogenesis of AHE is not fully understood, but the generally agreed concept links its development to astroglial cytotoxic oedema, caused by ammonia neurotoxicity (commonly known as "Trojan horse" hypothesis – (Albrecht and Norenberg, 2006)). Besides the contribution of hyperammoniemia to AHE, there is noted role of intestinal dysbiosis in patients with a long-term liver pathology, increased systemic LPS deriving from translocation of intestinal bacteria to the circulation, proinflammatory cytokines, and neurotransmitter imbalance (Aldridge et al., 2015; Shulyatnikova and Shavrin, 2017).

Astrocytes, the main homeostatic and defensive cells of the CNS (Verkhratsky and Nedergaard, 2018) form anatomical and functional barriers actively involved in the protection of brain parenchyma against extra-brain aggressive factors (Kubotera et al., 2019; Sofroniew, 2015; Zorec et al., 2019). In sepsis, astrocytes receive and integrate inflammatory signals connecting the immune system with brain parenchyma, thereby coordinating the neuroimmune response to systemic infection (Shulyatnikova and Verkhratsky, 2020). In ALF, associated with ammonium neurotoxicity, astroglia are one of the first and the major outposts in protecting the brain primarily by detoxifying ammonium and by compensating tissue oedema by regulating aqueous fluxes (Shulyatnikova and Shavrin, 2017).

Astrocytes interact with other nerve cells through the release of signalling molecules and are active contributors to the brain gliocrine system (Vardjan and Zorec, 2015; Verkhratsky et al., 2016). Release of neuroactive substances employs several pathways, of which exocytosis of secretory organelles, such as dense-core vesicles, synaptic-like microvesicles and extracellular vesicles (ECVs) is of particular importance (Vardjan et al., 2019). The cargo of ECVs includes various biologically active substances, such as mRNA, miRNA, signalling molecules, and cytokines (Liu et al., 2019; Turchinovich et al., 2019). Astrocytic ECVs are also associated with exocytosis of complement proteins C3a during neuroinflammation (Lian et al., 2015), and delivery of MHC-II molecules to the surface of reactive astrocytes acting as non-professional antigen presenting cells (Bozic et al., 2020; Vardjan et al., 2012).

Exosomes are one of the major types of ECVs, which are formed through the endosomal intracellular cycle from multivesicular bodies (MVBs) that fuse with the plasma membrane, thus releasing intraluminal vesicles (iLVs) into the extracellular space. The endosomal system is of paramount importance for interactions between the plasma membrane, the cellular synthesis-secretion apparatus and lysosomes. After endocytosis, transmembrane proteins are transported to the early endosomes, which undergo maturation and turn into iLVs of MVBs (late endosomes) (Huotari and Helenius, 2011). Intraluminal vesicles are formed by neutral sphingomyelinase-2 and a ceramide-dependent process (Trajkovic et al., 2008) involving also ESCRT-0, I, II, III (endosomal sorting complex required for transport) to form MVBs (Huotari and Helenius, 2011). These MVBs play a key role in sorting the products of intracellular metabolism - using the ESCRT mechanism they sequester membrane proteins and cytoplasmic molecules, which can subsequently translocate into lysosomes for catabolism (Luzio et al., 2010), or can be released as part of exosomes into the extracellular space (Doyle and Wang, 2019).

Systemic infection triggers astroglial reactivity, which is a fundamental part of the brain defence. Reactive astrocytes undergo disease-specific remodelling of their morphological, biochemical and secretory phenotype (Pekny et al., 2016). The status of astroglial endosomal system and MVB-exosomal secretion in systemic inflammatory endogenous intoxication has not been yet characterised. In the present paper, we employ two models of endogenous neurotoxicity, in particular: sepsis and acute liver failure, both of which lead to a rapid and profound toxic injury of the brain. We analysed the ultrastructure of reactive astrocytes and we found that systemic neurotoxicity triggers an increase in MVBs content and redistribution of MVBs to the perivascular astroglial processes.

2. Results

2.1. Histopathological characteristic of the CLP and AILF brains

2.1.1. CLP model

The ultrastructure of cortex and subcortical white matter was analysed in rats surviving for 24 h after CLP-procedure (compensated sepsis; n = 3) and in animals who did not survive for 24 h (decompensated sepsis; n = 7). In both groups, individual neurons at different stages of necrosis as well as small groups of necrotic neurons have been observed. In the "decompensated" group, these changes were more common and were found to exhibit partial disorganisation of nuclear components and cytoplasmic structures as well as partial destruction of organelles (Fig. 1A). Morphological signs of active consumption of intracellular substrates of energy metabolism, represented by significant e-translucency of cellular karyoplasm and hyaloplasm (Shavrin et al., 2008) were also frequently observed in cells (Fig. 1B). Astrocytes in "decompensated" CLP-animals compared to "compensated" ones were characterised by widespread signs of overhydration of the hyaloplasm, its increased translucency, vacuolisation, and focal decay, all seen in perivascular astrocytic endfeet (Fig. 1C) and parenchymal processes (Fig. 1D). Surrounding neuropil also showed signs of decompensated oedema and destructive processes of various degree. In the brains of "compensated" CLP-animals signs of activation of glial-neuronal interaction in the form of perineuronal oligodendroglial satellitosis (accumulation of glial cells encircling neurones) (Fig. 1E) were detected.

2.1.2. AILF model

In the compensated AILF model (n = 4), in 24 h after acetaminophen treatment, neurones at different stages of karyocytolysis were observed only sporadically, whereas in decompensated AILF (animals which did not survive 24 h) small groups of necrotic as well as neurons with signs of varying degrees of swelling (Fig. 2A) were routinely detected. Perineuronal satellitosis in the AILF-model was rare as compared with the CLP-model. In astrocytes of animals with decompensated AILF, pronounced signs of intracellular oedema with relatively more pronounced enlargement of astrocytic endfeet profiles and disorganisation with partial decay of most organelles were observed. The neuropil around them, and neighbouring other glial cells also combined varying degrees of common changes, indicating decompensation of tissue oedema (Fig. 2B, C).

2.2. MVBs morphology in astrocytes

Astrocytic MVBs were identified as vacuolar formations 0.4 μm to 1.2 μm in diameter which contained 2 to 30 iLVs with diameters ranging between 50 and >500 nm. MVBs in astrocytes were characterised by marked polymorphism. Thus, some of them contained a relatively high number of densely packed electron-transparent iLVs; whereas others presented large empty reservoirs with the residues of rarefied electron-dense substance or myelin-like bodies and other similar lamellar structures (Figs. 3A-B; 4A-E).

Astrocytes in control groups rarely contained MVBs (Table 1). These MVBs were equally distributed between three compartments analysed: astrocytic perikarya, astrocytic parenchymal processes and astrocytic capillary endfeet.

2.3. MVBs in astrocytes in Sepsis-Associative encephalopathy

The astroglia of survived animals from "CLP-A" group displayed indications of compensation of intracellular oedema in the form of extension of cytocavity network and greater preservation of cellular ultrastructural textures including plasma membrane. In these astrocytes, the number of MVBs was significantly increased compared to control group. The MVBs preferentially were accumulated in pericapillary astrocytic endfeet (Table 1, Fig. 4A). In the CLP-B animals, the

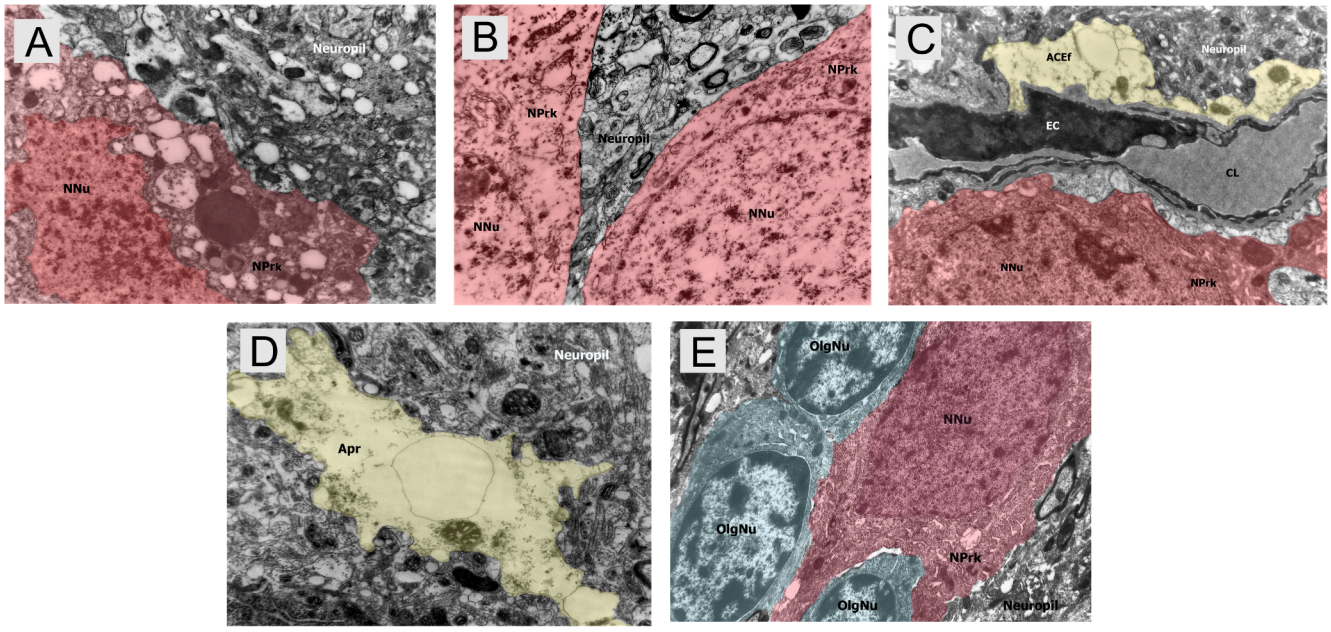

Fig. 1. Ultrastructural pathological changes of nervous tissue in sepsis-associated encephalopathy. A: Nuclear conformational changes with disintegration of chromatin and degenerative changes of the perikaryal ultrastructural textures observed in the neurone (shadowed in red) from CLP-B group. The cortex of a rat deceased due to decompensated sepsis. 20 h after CLP-procedure. TEM, mag. × 10,000. B: Significant e-translucency of the karyoplasm and hyaloplasm with slight vacuolisation of the cytoplasm – morphological signs of active consumption of intracellular energy substrates as seen in neurones shadowed in red from CLP-B group. The cortex of a rat deceased due to decompensated sepsis. 20 h after CLP-procedure. TEM, mag. × 12,000. C: Asymmetric pronounced oedema of the astroglial capillary endfeet in the cortex of a rat deceased due to decompensated sepsis (CLP-B group), with absence of MVBs. 22 h after CLP-procedure. TEM, mag. × 8,000. D: Decompensated oedema of the astroglial parenchymal process (without MVBs) in the cortex of a rat from CLP-B group. 23 h after CLP-procedure. TEM, mag. × 11,000. E: Oligodendroglial (shadowed in blue) satellitosis of the shadowed in red neurone signed by early stages of ischemic condensation in the cortex of a survived rat (CLP-A group). 24 h after CLP-procedure. TEM, mag. × 10,000. Abbreviations: NNu – neuronal nucleus; NPrk – neuronal perikaryon; ACEf – astroglial capillary endfeet shadowed in yellow; EC – endothelial cell; CL – capillary lumen; Apr – astroglial parenchymal process shadowed in yellow; OlgNu – oligodendroglial nucleus.

occurrence of MVBs also was found to be increased compared to control, however numbers of MVBs were smaller compared to the compensated cases of groups CLP-A (Table 1, Fig. 4B). Astrocytes containing MVBs in the perikaryon or in the processes were characterised by a relatively enhanced preservation of organelles and less pronounced cellular oedema (Fig. 4B).

2.4. MVBs in astrocytes in acute hepatic encephalopathy

The ultrastructural morphological parameters of MVBs in this model were identical to those in the CLP model. Astrocytes from animals with compensated AILF demonstrated activation of endosomal transport and intercellular interactions in a form of an increased number of MVBs. These astrocytes and surrounding neuropil were characterised by a relatively greater degree of ultrastructural preservation and lesser degree in severity of oedematous changes (Fig. 4C). The number of MVBs in astrocytes in AILF-A (compensated) group was higher than in AILF-B (decompensated) group and in control AILF-C group (Table 1, Fig. 4C, D). The highest number of MVBs was identified in capillary endfeet of astrocytes from AILF-A group. Astrocytes of animals who died in the conditions of decompensated AILF did not show differences in the number of MVBs in all their compartments with respect to the control group (Table 1, Fig. 4E).

2.5. Statistical analysis of MVBs occurrence in astroglial compartments

Statistical analysis of MVBs occurrence in astroglial compartments in control animals and in animals with compensated and decompensated pathology is presented in Fig. 5. Median values of MVBs numbers in all three studied compartments of astrocytes from both control groups were 0.00 (0.00; 1.00) MBVs/1 astrocytic profile.

In the CLP-A group the median values of MVBs numbers in the perikarya, in parenchymal processes and in capillary endfeet were, respectively: 2.00 (1.00; 3.00) units/1 profile; 1.00 (0.00; 2.00) units/1 profile; 3.00 (2.00; 4.00) units/1 profile; with a significant prevalence of the capillary endfeet indicators when comparing these 3 compartments ($p < 0.05$). The median values of MVBs numbers in capillary astrocytic endfeet at 24 h after surgery significantly exceeded numbers in the same compartments of control group by >3 times (respectively 3.00 (2.00; 4.00) units/1 profile and 0.00 (0.00; 1.00) units/1 profile; $p < 0.05$). The increased number of MVBs and their redistribution into capillary astrocytic endfeet is a hallmark of the astroglial ultrastructure in the group of surviving animals.

In the CLP-B group, the median values of MVBs numbers in astrocytic perikarya, parenchymal processes and capillary endfeet were: 1.00 (0.00; 2.00) units/1 profile; 1.00 (0.00; 1.00) units/1 profile; 1.00 (0.00; 1.00) units/1 profile, respectively. These values did not reach a significant difference compared to control group (0.00 (0.00; 1.00) units/1 profile, in all 3 studied profiles) ($p > 0.05$).

In the AILF-A group the median values of MVBs numbers in the perikarya, parenchymal processes and capillary endfeet, respectively, were: 1.00 (0.00; 1.50) units/1 profile; 0.50 (0.00; 1.00) units/1 profile; 2.00 (1.00; 3.00) units/1 profile; $p < 0.05$). Similarly, the median values of MVBs numbers in the astrocytic capillary endfeet from AILF-A group was significantly higher than in the same profiles of astrocytes in the AILF-B and AILF-C groups: 2.00 (1.00; 3.00) units/1 profile; 0.50 (0.00; 1.00) units/1 profile and 0.00 (0.00; 1.00) units/1 profile, respectively; $p < 0.05$).

In the AILF-B group, the median values of MVBs numbers in astrocytic perikarya, parenchymal processes and capillary endfeet were, respectively: 0.50 (0.00; 1.00) units/1 profile; 0.00 (0.00; 1.00) units/1 profile; 0.50 (0.00; 1.00) units/1 profile. These values did not reach significant difference compared to control group (0.00 (0.00; 1.00) units/1 profile, in all 3 studied profiles) ($p > 0.05$).

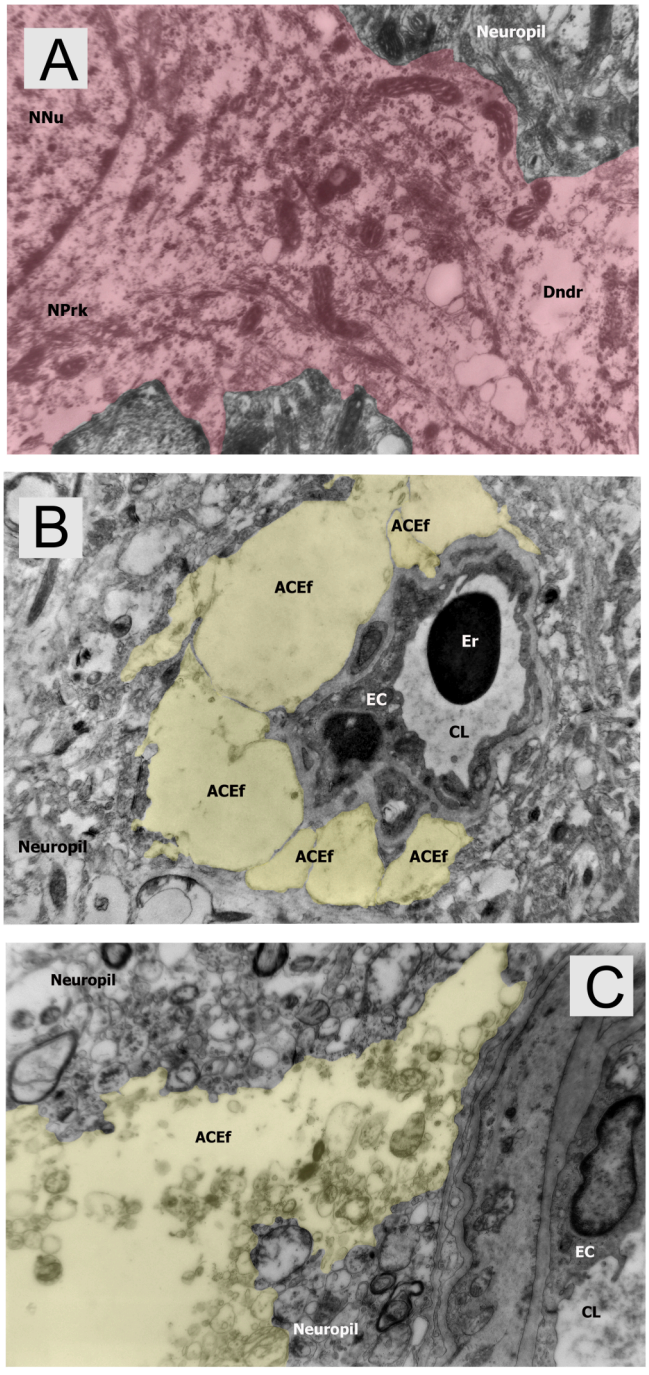

Fig. 2. Ultrastructural pathological changes of nervous tissue in acute hepatic encephalopathy. A: Neuronal (shadowed in red) swelling with partial disintegration of ultrastructural textures and plasmalemma as well as partial degenerative changes of the neuropil in the sensorimotor cortex of a rat from AILF-B group. 20 h after acetaminophen treatment. TEM, mag. × 16,000. B: Severe asymmetric oedema with absence of MVBs in the astrocytic capillary endfeet in the sensorimotor cortex of a rat from AILF-B group. 22 h after acetaminophen treatment. TEM, mag. × 10,000. C: Decompensated oedema of the vascular astrocytic endfeet with disintegration of ultrastructural textures and plasmalemma; signs of the decompensated oedematous surrounding neuropil. The cortex of a rat from AILF-B group. 23 h after acetaminophen treatment. TEM, mag. × 12,000. Abbreviations: NNu – neuronal nucleus; NPrk – neuronal perikaryon; Dndr – dendrite; ACEf – astroglial capillary endfeet shadowed in yellow; EC – endothelial cell; CL – capillary lumen; Er – erythrocyte.

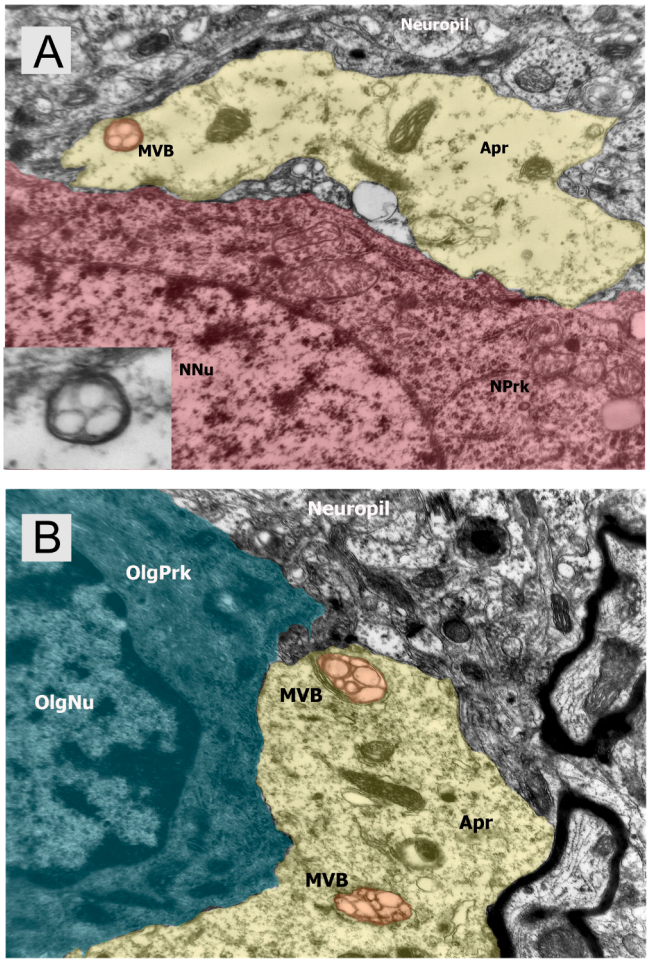

Fig. 3. Appearance of MVBs in astrocytes from control animals. A: The neurone shadowed in red and the adjacent parenchymal process of astrocyte with a single MVB. Insert shows the magnified image of MVB. The sensorimotor cortex of the control rat from AILF-C group. 24 h after procedure. TEM, mag. × 16,000. B: Oligodendrocyte shadowed in blue and the adjacent parenchymal process of astrocyte showing two MVBs in the cytoplasm of the astrocytic process. Border zone between cortex and white matter of the control rat from CLP-C group. 24 h after sham operation. TEM, mag. × 15,000. Abbreviations: NNu – neuronal nucleus; NPrk – neuronal perikaryon; Apr – astroglial parenchymal process shadowed in yellow; MVB – multivesicular body shadowed in orange; OlgNu – oligodendroglial nucleus; OlgPrk – oligodendroglial perikaryon.

Table 1
The number of MVBs in different compartments of astrocytes in the three groups of CLP & AILF models [expressed in the total number of MVBs (units)/total number of analysed compartments (units)]

Experimental models & subgroups	Perikarya	Parenchymal processes	Vascular endfeet
CLP-model			
CLP-A	201/90	99/90	273/90
CLP-B	217/210	133/210	154/210
CLP-C	70/150	45/150	75/150
AILF-model			
AILF-A	112/120	87/120	277/150
AILF-B	126/180	84/180	102/180
AILF-C	80/150	55/150	65/150

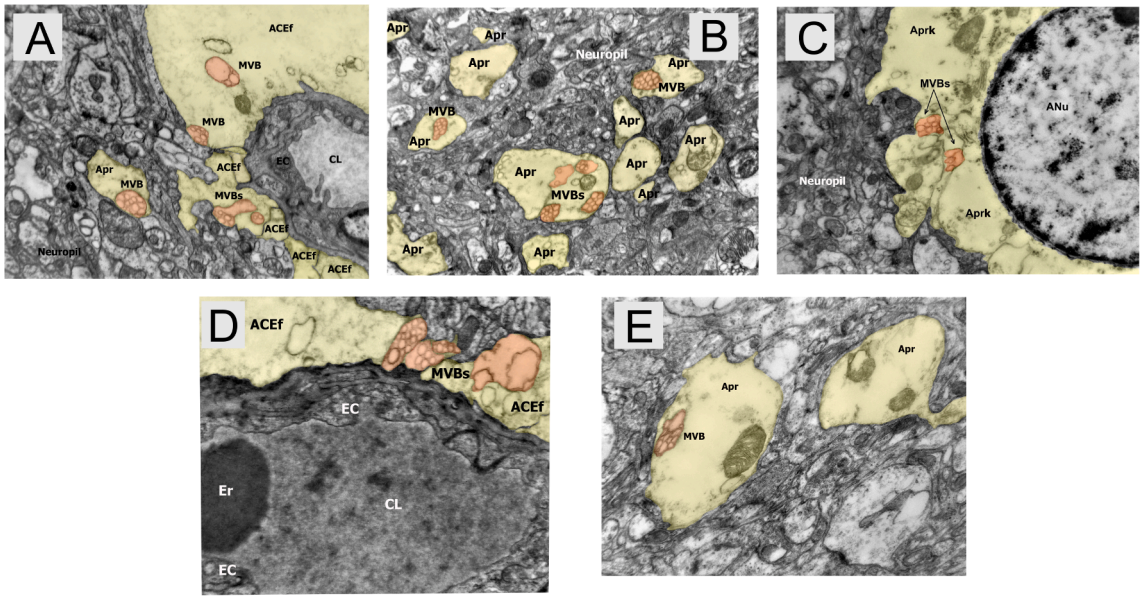

Fig. 4. The MVBs in astrocytes from animals with SAE and AHE. A: Accumulation of MVBs in the capillary astroglial endfeet in the sensorimotor cortex of the survived septic rat (CLP-A group). 24 h after CLP-procedure. TEM, mag. × 12,000. B: An increase in the number of MVBs in parenchymal astrocytic processes in the sensorimotor cortex of a rat deceased due to decompensated sepsis (CLP-B group). Surrounding neuropil with relatively normal appearing ultrastructure. 20 h after the CLP-procedure. TEM, mag. × 12,000. C: The slight swelling of the astrocytic perikaryon with the presence of two MVBs in the sensorimotor cortex of the survived rat in the condition of compensated AILF (AILF-A group). 24 h after acetaminophen treatment. TEM, mag. × 11,000. D: Accumulation of MVBs in the astroglial capillary endfeet in the sensorimotor cortex of the survived rat in the condition of the compensated AILF (AILF- A group). 24 h after acetaminophen treatment. TEM, mag. × 13,000. E: Formation of a single MVB in one of the astrocytic parenchymal processes. The sensorimotor cortex of a rat deceased due to decompensated AILF (AILF-B group). 23 h after acetaminophen treatment. TEM, mag. × 17,000. Abbreviations: MVB/MVBs – multivesicular body/bodies shadowed in orange; ACEf – astroglial capillary endfeet shadowed in yellow; EC – endothelial cell; CL – capillary lumen; Apr – astroglial parenchymal process shadowed in yellow; Aprk – astrocyte perikaryon shadowed in yellow; ANu – astrocytic nucleus; Er – erythrocyte.

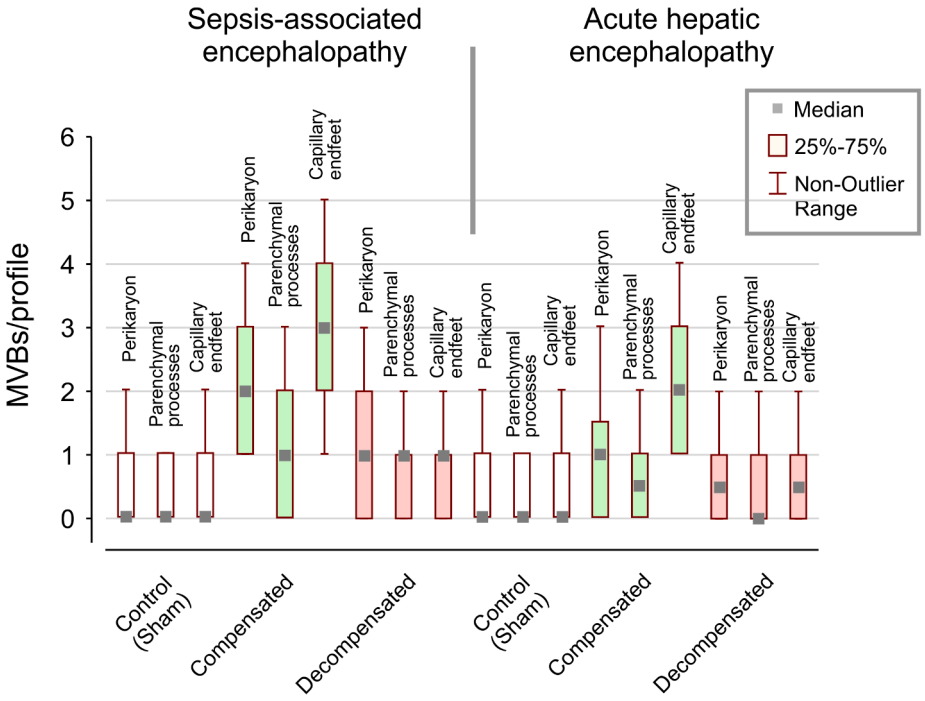

Fig. 5. Statistical analysis of MVBs occurrence in various astroglial compartments in SAE and AHE. Data are presented as median (Me) with lower and upper quartiles (Q1; Q3).

3. Discussion

The MVBs are formed because of endocytosis of small vacuolated parts of the surrounding neuropil and are the type of late endosomes. At different stages of their formation, they participate in various intracellular processes, interacting with other components of the cytocavity network and the lysosomal apparatus. This explains the relative polymorphism of MVBs, despite the constant presence of common

morphological characteristics.

In this paper, based on the ultrastructural analysis of astrocytes from the rat brains experiencing endogenous toxic encephalopathy, we demonstrated increase in numbers and accumulation of MVBs in astroglial perivascular endfeet and parenchymal processes. These changes were observed in two distinct models of toxic brain damage: the encephalopathy associated with sepsis and acute hepatic encephalopathy. Both models showed that in conditions of endogenous intoxication due to either systemic inflammation or acute liver failure, astrocytes undergo rapid reactive plasticity observed as an activation of their endosomal system. Importantly, these substantial changes in MVBs recruitment and endfeet accumulation were observed in animals with compensated form of encephalopathy. Redistribution and accumulation of astrocytic late endosomes in the pericapillary endfeet may indicate an increase in the blood–brain metabolism. In conditions of systemic inflammation, as well as in AILF, damaging factors cause functional impairment or anatomical damage to the CNS barriers, which in turn instigates the neuro-inflammatory response of the brain tissue (Donnelly et al., 2016; Shulyatnikova and Verkhratsky, 2020).

Neuroinflammation in sepsis, depending on the severity, is characterised by a spectrum of morphological changes, ranging from superficial and reversible alteration of intracellular and tissue metabolism of nervous tissue to severe circulatory disorders, decompensated oedema, purulent and necrotic processes (Shulyatnikova and Verkhratsky, 2020). While the pathological process remains compensated and homeostasis remains relatively preserved, we can presume activation of the defensive pathways to eliminate intracellular metabolic products by increasing endosomal-exosomal transport. Moreover, these changes indicate an increase in the activity of a special kind of gliocrine, signalling activity of astrocytes using exocytosis of molecules directly into the blood as a manifestation of the close relationship of brain metabolism and systemic reactions.

Several types of miRNAs, such as miR-155, miR-27b, miR-326, miR-124, miR-146a, miR-21, miR-223, let-7, transported by exosomes, can play a key role in the regulation of neuroinflammation, affecting glial inflammatory reactivity (Gaudet et al., 2018; Nuzziello and Liguori, 2019; Su et al., 2016). Systemic inflammation leads to an increase in number of MVBs and exosomes in the epithelium of the choroid plexus, which is associated with an increased level of ECV and pro-inflammatory miRNA in the cerebrospinal fluid. These exosomes, after penetrating the brain parenchyma, are captured by astrocytes and microglia, which upregulate glial pro-inflammatory genes and aggravate neuroinflammation (Balusu et al., 2016). Astrocytes, acting as conductors in the transmission of signalling molecules, may perform similar function through the contents of their exosomes thus regulating the inflammatory response of the brain tissue, as well as send signals to the periphery through blood and cerebrospinal fluid. Astrocytic exosomes also trigger apoptotic death of astrocytes. For example, amyloid peptide causes an increase in number of astrocytic exosomes containing PAR4 and ceramide (“apoxosomes”). These apoxosomes, reaching a pro-apoptotic concentration in the intercellular space, are subsequently captured by astrocytes and trigger an apoptosis by activation of caspase-3 (Wang et al., 2012). In conditions of neuroinflammation induced by sepsis or acute liver failure, apoptotic cell death is always present. The role of astroglia in these processes remains to be characterised.

There is also a close relationship between MVBs and autophagy processes as MVBs can merge with autophagosomes, forming dual “amphisome” organelles, which, in turn, unite with lysosomes and form autolysosomes to cleave the delivered products (Fader and Colombo, 2009). Effective autophagic degradation of certain proteins requires functionally active MVBs, and ESCRT mutations causing impaired synthesis of MVBs, are associated with a number of neurodegenerative diseases (Guo et al., 2018; Rusten and Simonsen, 2008). Thus, increase in number of astrocytic MVBs in neuroinflammation against the background of sepsis or liver failure may also indicate the activation of autophagy.

On the other hand, recent studies have shown the important role of astrocytic exosomes and their contents in glial-neuronal interaction in physiological and pathological conditions, where exosomes acted mainly as factors determining the survival and plasticity of neurones (Lafourcade et al., 2016; Pascua-Maestro et al., 2018). In our study, a relatively high number of MVBs in astrocytic parenchymal processes can indicate an increase in astro-astrocytic interaction and intensification of astrocytic endocytotic activity in perisynaptic compartments, which is natural during strengthened processes of dissociation, degradation and decay of synaptic apparatuses and are more typical for the animal brain in severe course of the disease. In surviving animals, morphological changes in astrocytic processes may indicate their active involvement in the mechanisms of synaptic plasticity during adaptation to acute hypoxia, intoxication and oedema, which are observed in SAE and AHE. Perisynaptic astrocytic processes form the “synaptic cradle” (Verkhratsky and Nedergaard, 2014), which maintains homeostasis in the synaptic cleft and sustained neurotransmission; impairment of this structure may result in neurotransmitter imbalance, which is observed in SAE and AHE (Shulyatnikova and Shavrin, 2017; van Gool et al., 2010).

According to the results of our study, the ultrastructural morphology of astrocytic reactivity in Wistar laboratory rats under septic and liver failure conditions display similar stereotype, which indicates a certain algorithm of structural and functional transformations in astrocytes in response to systemic endogenous intoxication. A number of common links have been identified in the pathogenesis of SAE and AHE. In particular, substantial cytokine imbalance and development of neuroinflammation are key damaging mechanisms realised directly inside the brain environment (Donnelly et al., 2016). An explanation for the similarity of astrocytic reaction in the models employed is that acute liver failure is a frequent component of sepsis, especially its severe forms, which can be reproduced in the CLP-model. In sepsis, acute liver failure of varying severity is often part or even a primary component of MODS (Wang et al., 2014). Our study revealed some differences between astrocytic reaction to ALF caused by acetaminophen poisoning, and the complex effect of toxins on the brain during abdominal sepsis. In the latter, a high level of lipopolysaccharide and “cytokine storm” exert a greater damaging effect on the CNS than hyperammoniemia and neurotransmitter imbalance. In addition, the relative imperfection of the ALF model can be a reason for the differences, where it is necessary to take into account the specific properties of acetaminophen itself as an exogenous chemical substance that has an ambiguous effect on the body systems (Mossanen and Tacke, 2015).

Astroglial reactivity, discovered to develop in various forms of brain pathology a century ago (Del Río-Hortega and Penfield, 1927) remains an actively discussed matter. Several simple approaches, subdividing reactive astrocytes into main types - proliferative and non-proliferative or neuroprotective and neurotoxic – failed to describe the broad spectrum of morpho-functional transformations resulting in multiple, and often disease-specific, reactive phenotypes (Verkhratsky et al., 2017). Astroglial reactive transformations are manifested by changes in cellular morphology, proliferative activity, molecular expression, cellular interactions and selective changes in the transcriptome of groups of specific astrocytic subtypes or individual cells (Sofroniew, 2020). Ultrastructural analysis of reactive astrocytes represents even more complex problem. The main ultrastructural changes associated with astroglial reactivity are: (i) an increase number of glycogen granules and mitochondria; (ii) accumulation of lipid bodies and cytoplasmic fibrils (iii) cellular swelling and hypertrophy and (iv) dilation in the endoplasmic reticulum and increased gliofilaments (Maxwell and Kruger, 1965; Castejon, 2013). Reactive changes in astroglial endosomal apparatus in conditions of systemic inflammation have been rarely explored. Recently, activation of astrocytic lysosomal exocytosis leading to major histocompatibility complex class II-linked antigen surface presentation on reactive astrocytes has been demonstrated, albeit no ultrastructural analysis has been performed (Bozic et al., 2020). Our study therefore shows, for the first time, subcellular manifestations of the early

structural reorganisation of reactive astrocytes, combined with general tissue remodelling related to beneficial outcome of the encephalopathy and the animal survival. These ultrastructural changes of astroglial endosomal system can, arguably, represent a general feature of astrocytic reactivity in response to acute endogenous intoxication.

During reactive changes in response to systemic toxicity, astrocytes can follow at least two different scenarios. Under favourable conditions, they actively rebuild their ultrastructure, activating the mechanisms of intracellular transport and secretion, while adjusting general orientation of tissue reaction in direction of restoring impaired homeostasis. Under unfavourable conditions, astroglia rapidly expend homeostatic potential and are subjected to increased hydration and disintegration of intracellular ultrastructure, which lead to their partial or complete functional failure and cause decompensation of the tissue pathology (Fig. 6). These two sets of glial responses clearly show an activation of endosomal system in compensated pathology and its failure in the decompensated pathology leading to rapid death.

4. Conclusion

In conditions of endogenous intoxication caused by either systemic inflammation or acute liver failure, rapid emergence of reactive changes are observed in astrocytes; these changes are manifest with an increase in the activity of astrocytic endosomal-exosomal apparatus, which reflects adaptive astroglial remodelling aimed at compensation of the pathology. In particular, these changes are translated into an increased number of late endosomes – multivesicular bodies, – which predominantly accumulate in the capillary astrocytic endfeet. Accumulation of MVBs in astrocytic processes may indicate the activation of glial-glial, glial-neuronal, neuro-glial, glial-vascular interaction through endo- and exocytosis in the acute phase of adaptive processes in sepsis-associated and acute hepatic encephalopathy. There is also a certain stereotype of reactive astroglial changes in systemic inflammation and acute liver failure, which indicates an activation of similar reactive program.

5. Materials and methods

5.1. Animals

The study was conducted on the male Wistar rats, 200–300 g (obtained from the PE “Biomodelservice”, Kiev, The Ukraine). Animals were kept in acrylic cages (5 animals per cage) under a 12-h light–dark cycle, at 22 °C ± 2 °C, with free access to food (standard chow for rats, PE “Biomodelservice”, Kiev, The Ukraine) and water. Acclimatisation for the animals prior to experimental procedures was provided for one week. All procedures were performed in accordance with the “Guide for the care and use of laboratory animals” (National Research Council (US) Committee for the Update of the Guide for the Care and Use of Laboratory Animals. Guide for the Care and Use of Laboratory Animals. 8th edition. Washington (DC): National Academies Press; 2011), European Convention for the Protection of Vertebrate Animals Used for Experimental and other Scientific Purposes (Strasbourg, 18 March 1986; ETS №123), the Directive 2010/63/EU on the protection of animals used for scientific purposes and also was approved by the Commission on Bioethics of Zaporizhzhia State Medical University.

5.2. Sepsis-associated encephalopathy model

Animals were subjected to the cecal ligation and puncture (CLP) model of sepsis, which is widely used to induce experimental polymicrobial abdominal sepsis in rodents (Rittirsch et al., 2009; Toscano et al., 2011). Animals were randomly divided into 2 groups: control group (sham-operated rats, n = 5) and experimental CLP group (n = 10). Animals were anesthetised by intraperitoneal (i.p.) injection of ketamine hydrochloride (50 mg/mL; Ketamine, Farmak, The Ukraine) 80 mg/kg and xylazine hydrochloride (20 mg/mL; Xylazine, Alfasan, The Netherlands) 10 mg/kg. After anaesthesia, under aseptic conditions, a 3 cm longitudinal midline laparotomy was performed and cecum was mobilised. After dissection of the mesentery, cecum was tightly ligated with a 3.0-silk suture below the ileocecal valve (without causing bowel obstruction). The ratio of the ligated part to the conditionally intact part of the intestine (from the ligature to the ileocecal valve) was 75%:25%, which triggers severe sepsis (Rittirsch et al., 2009). Next, the ligated part of the cecum was perforated with an 18 G needle and a small amount of

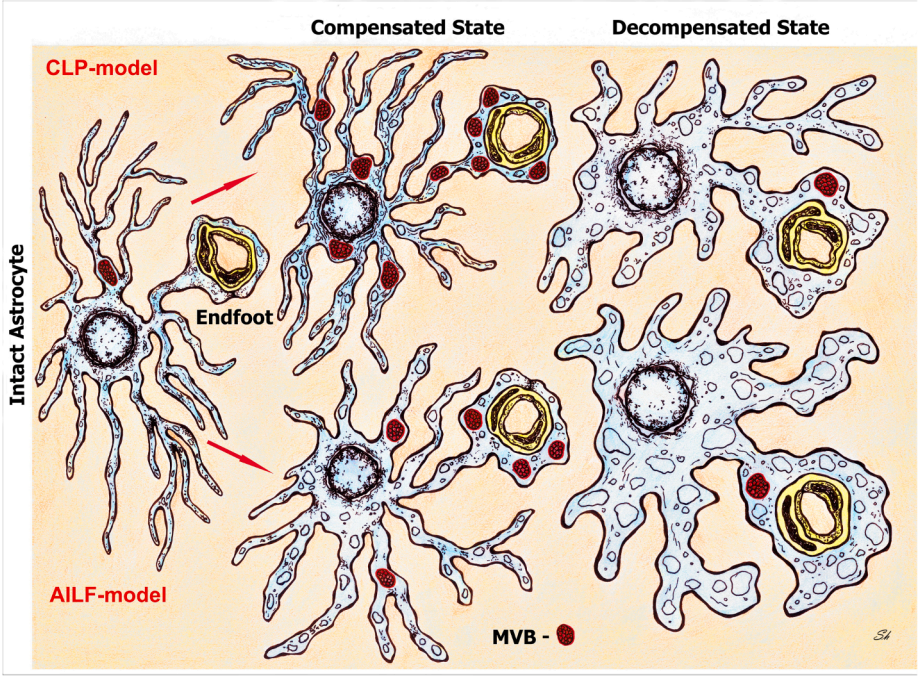

Fig. 6. MVBs as a part of reactive responses of astroglia to endogenous toxic encephalopathy. The scheme shows the activation of the endosomal system in astrocytes undergoing reactive changes in response to CLP and AILF models of sepsis-associated encephalopathy and acute hepatic encephalopathy. In compensated state of the tissue pathology, in astrocytes, the numbers of MVB rises significantly and are redistributed to endfeet, arguably for subsequent exocytosis. In a decompensated state MVBs are depleted, which possibly reflects exhaustion of astrocytic defensive mechanisms.

faecal contents was extruded into the abdominal cavity from the punctured sites. Then the intestine was replaced to the peritoneal cavity and the abdominal wall was closed using two layers of sterile silk sutures. In the control group of sham-operated animals, the same procedures were carried out, but without ligation and perforation of the cecum. All animals immediately after the operation were resuscitated by subcutaneous injection of physiological saline, previously heated to 37 °C (5 ml/100 g). In the postoperative period, animals were kept in cages, under the same conditions as before the operation, with free access to food and water. Postoperatively, at first 2 h animals were observed every 30 min and then – every 6 h up to 24 h after the CLP procedure. The following signs were evaluated: lethargy, diarrhoea, fever/hypothermia, piloerection, periorbital exudation, respiratory disorders, social isolation, huddling and malaise. At the period up to 24 h after the operation in the CLP group of 10 animals, 3 animals survived until the end of the experiment (group "CLP-A" – compensated sepsis), 7 rats showed severe clinical signs of sepsis and were euthanised (group "CLP-B" – decompensated sepsis); in the control group (group "CLP-C") there were no deceased animals. 24 h after the operation, all survived and control animals were euthanised by intraperitoneal administration of sodium thiopental euthanasia solution (100 mg/mL; Thiopental, Arterium, The Ukraine) 60 mg/kg.

5.3. Acute hepatic encephalopathy model

For induction of acute hepatic encephalopathy (AHE) type "A" ("Acute liver failure" – according to the American Association for the Study of Liver Disease (AASLD) updated guidelines, (Vilstrup et al., 2014)) we used acetaminophen (paracetamol, N-acetyl-p-aminophenol [APAP])-induced liver failure (AILF) model (McGill et al., 2012; Mossanen and Tacke, 2015). Acetaminophen is the most widely used antipyretic and/or analgesic drug. Overdosing acetaminophen is the primary cause of ALF in many countries, determining more than half of all cases in the USA (Mitchell et al., 2020). Due to the fact, that acetaminophen overdosing also causes ALF in rats this model can be used for analysing mechanisms of acute hepatic encephalopathy similar to that in humans.

Paracetamol (Paracetamol-Darnitsa, "Darnitsa", The Ukraine) was dissolved in 0.9% sodium chloride (NaCl 0.9%) at 15 mg/mL, at 30 °C in a water bath. Animals were randomly divided into 2 groups: control group (n = 5) and AILF-group (n = 10). Before inducing AILF, rats were fasted with free access to water during 12 h to create comparable conditions for acetaminophen catabolism. Then rats were weighed and i.p. injected into the lower side of the abdomen with acetaminophen solution at 1.5 g/kg body weight. The control group of rats received i.p. equivalent volume of 0.9% sodium chloride.

The indicated dose selected for the AILF procedure was based on previous studies (McGill et al., 2012) and leads to significant liver damage permitting however significant animal survival in the first 24 h after AILF induction. The effectiveness of the model was confirmed by the clinical symptoms of acute liver failure, such as altered behaviour, major physiological parameters, and decreased level of consciousness in animals. Histopathological manifestations of acute liver damage were represented by centrolobular coagulative necrosis and severe dystrophic changes of hepatocytes in all studied cases. To determine the latter, liver tissue was fixed in 10% neutral-buffered formalin, embedded in paraffin, sliced into 4 μm-thick sections, and stained with hematoxylin and eosin. Mentioned morphological characteristics were evaluated after studying the sections at the light-optical level.

After AILF, free access to standard chow diet was allowed. Rats were examined every 1 h during first 12 h and after – every 0.5 h for signs of changed respiration and heart rate, lethargy, weakness, and hypothermia. Six rats were euthanised up to 24 h from the initiation of the experiment; euthanasia was achieved by an i.p. administration of sodium thiopental euthanasia solution (100 mg/mL; Thiopental, Arterium, The Ukraine) 60 mg/kg due to the above severe clinical symptoms. Animals that survived up to 24 h after the procedure (4 rats) were designated to group "AILF-A" – compensated AILF; 6 animals which died within 24 h after procedure constituted the group "AILF-B" – decompensated AILF). In the control group "AILF-C", all five animals survived over 24 h. In 24 h after AILF-procedure, all survived and control animals were euthanised via intraperitoneal injection of euthanasia solution of sodium thiopental.

5.4. Tissue preparation for transmission electron microscopy (TEM)

Brains were removed immediately after stopping the heartbeat and placed at 25 °C in a standard fixation solution for TEM (up to 5 min - before tissue blocks were taken): 2.5% glutaraldehyde (Alfa Aesar by Thermo Fisher Scientific, A17876) in 0.1 M phosphate buffer, pH = 7.4. Blocks up to 1x1x1 mm were cut from the sensorimotor cortex of the frontal lobe of the left hemisphere and placed for 2 h (at t = 4 °C) in the same fixation solution with the addition of sucrose. Additional fixation for 2 h was performed using 1% osmium tetroxide in phosphate buffer at 4 °C. Specimens were next processed through graded (up to 100%) series of ethanol for dehydration and stained by 2.5% ethanolic uranyl acetate solution for 2 h at 4 °C. Dehydrated specimens were then infiltrated with a mixture of acetone and Epon resin (2:1; 1:1; 1:2), embedded in epoxy medium Epon-812 (Sigma-Aldrich Chemie, GmbH, Taufkirchen, Germany, 45345) and polymerised in two steps: at 36 °C (12 h); and 56 °C (24 h). Semithin (1–2 μm) and ultrathin (55–65 nm) sections were cut using the ultramicrotome (PowerTome RMC Boeckeler, USA) and stained by lead citrate according to Reynolds (30 min, t = 25 °C). Semithin sections were stained by methylene blue and basic fuchsin (Aparicio and Marsden, 1969). Examination of ultrathin sections at different magnifications and acquiring of images were carried out with a PEM-100–01 electron microscope ("Selmi", Sumy, The Ukraine) at 65 kV.

5.5. Statistical analysis

While studying tissue sections from each animal in TEM we analysed the ultrastructure of astrocytic perikarya, "parenchymal" processes (i.e. those not associated with capillary endfeet) and capillary endfeet profiles. From each animal 5 blocks of tissue were examined; from each block stepped (every fourth) ultrathin sections (with an area of ~3500 μm^2 each) were cut. Thirty units of each of the astrocytic profiles indicated above were selected and constituted the basis of final calculation of MVBs-numbers in their composition.

Data were analysed using the package of Statistica® for Windows 13.0 (StatSoft Inc., license N№ JPZ804I382130ARCN10-J). The median (Me), the lower and upper quartiles (Q1; Q3) were calculated; the comparison between two groups of observations was carried out using the Mann-Whitney *U* test, between three or more groups of observations – using the Kruskal-Wallis Test. The results were considered statistically significant at 95% ($p < 0.05$).

6. Author's contributions

The authors have contributed equally to the manuscript.

Funding

This study was conducted in the framework of the scientific research work of Zaporizhzhia State Medical University "The morphogenesis of destructive-reparative processes of the brain in the diseases of vascular and toxic-metabolic origin", N№ of state registration 0118U004253 (2018–2022) of the Ministry of Health of Ukraine.

CRediT authorship contribution statement

Tatyana Shulyatnikova: Conceptualization, Methodology,

Investigation, Formal analysis, Visualization, Writing - original draft. **Vladimir Shavrin:** Conceptualization, Methodology, Investigation, Visualization, Writing - review & editing, Supervision.

Declaration of Competing Interest

The authors declare that they have no known competing financial interests or personal relationships that could have appeared to influence the work reported in this paper.

Appendix A. Supplementary data

Supplementary data to this article can be found online at https://doi.org/10.1016/j.brainres.2020.147174.

References

Albrecht, J., Norenberg, M.D., 2006. Glutamine: a Trojan horse in ammonia neurotoxicity. Hepatology 44, 788–794.
Aldridge, D.R., Tranah, E.J., Shawcross, D.L., 2015. Pathogenesis of hepatic encephalopathy: role of ammonia and systemic inflammation. J. Clin. Exp. Hepatol. 5, S7–S20.
Aparicio, S.R., Marsden, P., 1969. A rapid methylene blue-basic fuchsin stain for semi-thin sections of peripheral nerve and other tissues. J. Microsc. 89, 139–141.
Balusu, S., Van Wonterghem, E., De Rycke, R., Raemdonck, K., Stremersch, S., Gevaert, K., Brkic, M., Demeestere, D., Vanhooren, V., Hendrix, A., Libert, C., Vandenbroucke, R.E., 2016. Identification of a novel mechanism of blood-brain communication during peripheral inflammation via choroid plexus-derived extracellular vesicles. EMBO Mol. Med. 8, 1162–1183.
Bozic, M., Verkhratsky, A., Zorec, R., Stenovec, M., 2020. Exocytosis of large-diameter lysosomes mediates interferon gamma-induced relocation of MHC class II molecules toward the surface of astrocytes. Cell. Mol. Life Sci. 77, 3245–3264.
Brown, G.C., 2019. The endotoxin hypothesis of neurodegeneration. J. Neuroinflammation 16, 180.
Castejon, O.J., 2013. Electron microscopy of astrocyte changes and subtypes in traumatic human edematous cerebral cortex: a review. Ultrastruct. Pathol. 37, 417–424.
Del Río-Hortega, P., Penfield, W.G., 1927. Cerebral cicatrix: The reaction of neuroglia and microglia to brain wounds. Bull. John Hopkins Hosp. 41, 278–303.
Donnelly, M.C., Hayes, P.C., Simpson, K.J., 2016. Role of inflammation and infection in the pathogenesis of human acute liver failure: Clinical implications for monitoring and therapy. World J. Gastroenterol. 22, 5958–5970.
Doyle, L.M., Wang, M.Z., 2019. Overview of extracellular vesicles, their origin, composition, purpose, and methods for exosome isolation and analysis. Cells 8.
Fader, C.M., Colombo, M.I., 2009. Autophagy and multivesicular bodies: two closely related partners. Cell Death Differ. 16, 70–78.
Gaudet, A.D., Fonken, L.K., Watkins, L.R., Nelson, R.J., Popovich, P.G., 2018. MicroRNAs: roles in regulating neuroinflammation. Neuroscientist 24, 221–245.
Guo, F., Liu, X., Cai, H., Le, W., 2018. Autophagy in neurodegenerative diseases: pathogenesis and therapy. Brain Pathol. 28, 3–13.
Huotari, J., Helenius, A., 2011. Endosome maturation. EMBO J. 30, 3481–3500.
Jain, L., Sharma, B.C., Sharma, P., Srivastava, S., Agrawal, A., Sarin, S.K., 2012. Serum endotoxin and inflammatory mediators in patients with cirrhosis and hepatic encephalopathy. Dig. Liver Dis. 44, 1027–1031.
Kubotera, H., Ikeshima-Kataoka, H., Hatashita, Y., Allegra Mascaro, A.L., Pavone, F.S., Inoue, T., 2019. Astrocytic endfeet re-cover blood vessels after removal by laser ablation. Sci. Rep. 9, 1263.
Lafourcade, C., Ramirez, J.P., Luarte, A., Fernandez, A., Wyneken, U., 2016. MiRNAs in astrocyte-derived exosomes as possible mediators of neuronal plasticity. J. Exp. Neurosci. 10, 1–9.
Lamar, C.D., Hurley, R.A., Taber, K.H., 2011. Sepsis-associated encephalopathy: review of the neuropsychiatric manifestations and cognitive outcome. J. Neuropsychiatry Clin. Neurosci. 23, 237–241.
Lian, H., Yang, L., Cole, A., Sun, L., Chiang, A.C., Fowler, S.W., Shim, D.J., Rodriguez-Rivera, J., Taglialatela, G., Jankowsky, J.L., Lu, H.C., Zheng, H., 2015. NFκB-activated astroglial release of complement C3 compromises neuronal morphology and function associated with Alzheimer's disease. Neuron 85, 101–115.
Liu, T., Zhang, Q., Zhang, J., Li, C., Miao, Y.R., Lei, Q., Li, Q., Guo, A.Y., 2019. EVmiRNA: a database of miRNA profiling in extracellular vesicles. Nucleic Acids Res. 47, D89–D93.
Luzio, J.P., Gray, S.R., Bright, N.A., 2010. Endosome-lysosome fusion. Biochem. Soc. Trans. 38, 1413–1416.
Maxwell, D.S., Kruger, L., 1965. The Fine structure of astrocytes in the cerebral cortex and their response to focal injury produced by heavy ionizing particles. J. Cell Biol. 25, 141–157.
McGill, M.R., Williams, C.D., Xie, Y., Ramachandran, A., Jaeschke, H., 2012. Acetaminophen-induced liver injury in rats and mice: comparison of protein adducts, mitochondrial dysfunction, and oxidative stress in the mechanism of toxicity. Toxicol. Appl. Pharmacol. 264, 387–394.
Mitchell, R.A., Rathi, S., Dahiya, M., Zhu, J., Hussaini, T., Yoshida, E.M., 2020. Public awareness of acetaminophen and risks of drug induced liver injury: Results of a large outpatient clinic survey. PLoS ONE 15, e0229070.
Montrief, T., Koyfman, A., Long, B., 2019. Acute liver failure: a review for emergency physicians. Am. J. Emerg. Med. 37, 329–337.
Mossanen, J.C., Tacke, F., 2015. Acetaminophen-induced acute liver injury in mice. Lab. Anim. 49, 30–36.
Munoz, S.J., 2014. Complications of acute liver failure. Gastroenterol. Hepatol. (N. Y.) 10, 665–668.
Nuzziello, N., Liguori, M., 2019. The MicroRNA centrism in the orchestration of neuroinflammation in neurodegenerative diseases. Cells 8, 8101193.
Pascua-Maestro, R., Gonzalez, E., Lillo, C., Ganfornina, M.D., Falcon-Perez, J.M., Sanchez, D., 2018. Extracellular vesicles secreted by astroglial cells transport apolipoprotein D to neurons and mediate neuronal survival upon oxidative stress. Front. Cell. Neurosci. 12, 526.
Pekny, M., Pekna, M., Messing, A., Steinhauser, C., Lee, J.M., Parpura, V., Hol, E.M., Sofroniew, M.V., Verkhratsky, A., 2016. Astrocytes: a central element in neurological diseases. Acta Neuropathol. 131, 323–345.
Rittirsch, D., Huber-Lang, M.S., Flierl, M.A., Ward, P.A., 2009. Immunodesign of experimental sepsis by cecal ligation and puncture. Nat. Protoc. 4, 31–36.
Ronco, C., Piccinni, P., Rosner, M.H. (Eds.), 2010. Endotoxemia and Endotoxin Shock: Disease, Diagnosis and Therapy. Contributions to Nephrology. Karger, Basel.
Rusten, T.E., Simonsen, A., 2008. ESCRT functions in autophagy and associated disease. Cell Cycle 7, 1166–1172.
Sartelli, M., Abu-Zidan, F.M., Catena, F., Griffiths, E.A., Di Saverio, S., Coimbra, R., Ordonez, C.A., Leppaniemi, A., Fraga, G.P., Coccolini, F., Agresta, F., Abbas, A., Abdel Kader, S., Agboola, J., Amhed, A., Ajibade, A., Akkucuk, S., Alharthi, B., Anyfantakis, D., Augustin, G., Baiocchi, G., Bala, M., Baraket, O., Bayrak, S., Bellanova, G., Beltran, M.A., Bini, R., Boal, M., Borodach, A.V., Bouliaris, K., Branger, F., Brunelli, D., Catani, M., Che Jusoh, A., Chichom-Mefire, A., Cocorullo, G., Colak, E., Costa, D., Costa, S., Cui, Y., Curca, G.L., Curry, T., Das, K., Delibegovic, S., Demetrashvili, Z., Di Carlo, I., Drozdova, N., El Zalabany, T., Enani, M.A., Faro, M., Gachabayov, M., Gimenez Maurel, T., Gkiokas, G., Gomes, C. A., Gonsaga, R.A., Guercioni, G., Guner, A., Gupta, S., Gutierrez, S., Hutan, M., Ioannidis, O., Isik, A., Izawa, Y., Jain, S.A., Jokubauskas, M., Karamarkovic, A., Kauhanen, S., Kaushik, R., Kenig, J., Khokha, V., Kim, J.I., Kong, V., Koshy, R., Krasniqi, A., Kshirsagar, A., Kuliesius, Z., Lasithiotakis, K., Leao, P., Lee, J.G., Leon, M., Lizarazu Perez, A., Lohsiriwat, V., Lopez-Tomassetti Fernandez, E., Lostoridis, E., Mn, R., Major, P., Marinis, A., Marrelli, D., Martinez-Perez, A., Marwah, S., McFarlane, M., Melo, R.B., Mesina, C., Michalopoulos, N., Moldovanu, R., Mouaqit, O., Munyika, A., Negoi, I., Nikolopoulos, I., Nita, G.E., Olaoye, I., Omari, A., Ossa, P.R., Ozkan, Z., Padmakumar, R., Pata, F., Pereira Junior, G.A., Pereira, J., Pintar, T., Pouggouras, K., Prabhu, V., Rausei, S., Rems, M., Rios-Cruz, D., Sakakushev, B., Sanchez de Molina, M.L., Seretis, C., Shelat, V., Simoes, R.L., Sinibaldi, G., Skrovina, M., Smirnov, D., Spyropoulos, C., Tepp, J., Tezcaner, T., Tolonen, M., Torba, M., Ulrych, J., Uzunoglu, M.Y., van Dellen, D., van Ramshorst, G.H., Vasquez, G., Venara, A., Vereczkei, A., Vettoretto, N., Vlad, N., Yadav, S.K., Yilmaz, T.U., Yuan, K.C., Zachariah, S.K., Zida, M., Zilinskas, J., Ansaloni, L., 2015. Global validation of the WSES Sepsis Severity Score for patients with complicated intra-abdominal infections: a prospective multicentre study (WISS Study). World J. Emerg. Surg. 10, 61.
Shavrin, V.A., Shulyatnikova, T., Polkovnikov, Y.F., 2008. Morphogenesis of the "ischaemic-homogenizing" neuronal changes and their significance in the pathohistological diagnostics of ischaemic diseases of the brain. Patologia 5 (4), 73–78.
Shuliatnikova, T.V., Shavrin, V.O., 2018. Sepsis associated encephalopathy and abdominal sepsis: current state of problem. Art Med. 3, 158–165.
Shulyatnikova, T., Verkhratsky, A., 2020. Astroglia in sepsis associated encephalopathy. Neurochem. Res. 45, 83–99.
Shulyatnikova, T.V., Shavrin, V.A., 2017. Modern view on hepatic encephalopathy: basic terms and concepts of pathogenesis. Pathologia 14, 371–380.
Sofroniew, M.V., 2015. Astrocyte barriers to neurotoxic inflammation. Nat. Rev. Neurosci. 16, 249–263.
Sofroniew, M.V., 2020. Astrocyte reactivity: subtypes, states, and functions in CNS innate immunity. Trends Immunol. 41, 758–770.
Sonneville, R., Verdonk, F., Rauturier, C., Klein, I.F., Wolff, M., Annane, D., Chretien, F., Sharshar, T., 2013. Understanding brain dysfunction in sepsis. Ann. Intensive Care 3, 15.
Su, W., Aloi, M.S., Garden, G.A., 2016. MicroRNAs mediating CNS inflammation: Small regulators with powerful potential. Brain Behav. Immun. 52, 1–8.
Toscano, M.G., Ganea, D., Gamero, A.M., 2011. Cecal ligation puncture procedure. J Vis Exp 7, 2860.
Trajkovic, K., Hsu, C., Chiantia, S., Rajendran, L., Wenzel, D., Wieland, F., Schwille, P., Brugger, B., Simons, M., 2008. Ceramide triggers budding of exosome vesicles into multivesicular endosomes. Science 319, 1244–1247.
Turchinovich, A., Drapkina, O., Tonevitsky, A., 2019. Transcriptome of extracellular vesicles: state-of-the-art. Front. Immunol. 10, 202.
van Gool, W.A., van de Beek, D., Eikelenboom, P., 2010. Systemic infection and delirium: when cytokines and acetylcholine collide. Lancet 375, 773–775.
Vardjan, N., Gabrijel, M., Potokar, M., Svajger, U., Kreft, M., Jeras, M., de Pablo, Y., Faiz, M., Pekny, M., Zorec, R., 2012. IFN-γ-induced increase in the mobility of MHC class II compartments in astrocytes depends on intermediate filaments. J. Neuroinflammation 9, 144.
Vardjan, N., Parpura, V., Verkhratsky, A., Zorec, R., 2019. Gliocrine System: Astroglia as secretory cells of the CNS. Adv. Exp. Med. Biol. 1175, 93–115.
Vardjan, N., Zorec, R., 2015. Excitable astrocytes: Ca^{2+}- and cAMP-regulated exocytosis. Neurochem. Res. 40, 2414–2424.
Verkhratsky, A., Zorec, R., Parpura, V., 2017. Stratification of astrocytes in healthy and diseased brain. Brain Pathol. 27, 629–644.

Verkhratsky, A., Matteoli, M., Parpura, V., Mothet, J.P., Zorec, R., 2016. Astrocytes as secretory cells of the central nervous system: idiosyncrasies of vesicular secretion. EMBO J. 35, 239–257.

Verkhratsky, A., Nedergaard, M., 2014. Astroglial cradle in the life of the synapse. Philos. Trans. R. Soc. Lond. B Biol. Sci. 369, 20130595.

Verkhratsky, A., Nedergaard, M., 2018. Physiology of astroglia. Physiol. Rev. 98, 239–389.

Vilstrup, H., Amodio, P., Bajaj, J., Cordoba, J., Ferenci, P., Mullen, K.D., Weissenborn, K., Wong, P., 2014. Hepatic encephalopathy in chronic liver disease: 2014 Practice Guideline by the American Association for the Study of Liver Diseases and the European Association for the Study of the Liver. Hepatology 60, 715–735.

Wang, D., Yin, Y., Yao, Y., 2014. Advances in sepsis-associated liver dysfunction. Burns Trauma 2, 97–105.

Wang, G., Dinkins, M., He, Q., Zhu, G., Poirier, C., Campbell, A., Mayer-Proschel, M., Bieberich, E., 2012. Astrocytes secrete exosomes enriched with proapoptotic ceramide and prostate apoptosis response 4 (PAR-4): potential mechanism of apoptosis induction in Alzheimer disease (AD). J. Biol. Chem. 287, 21384–21395.

Zorec, R., Zupanc, T.A., Verkhratsky, A., 2019. Astrogliopathology in the infectious insults of the brain. Neurosci. Lett. 689, 56–62.